

RGBD-GAN: UNSUPERVISED 3D REPRESENTATION LEARNING FROM NATURAL IMAGE DATASETS VIA RGBD IMAGE SYNTHESIS

Atsuhiko Noguchi¹ & Tatsuya Harada^{1,2}

¹The University of Tokyo, ²RIKEN

{noguchi, harada}@mi.t.u-tokyo.ac.jp

ABSTRACT

Understanding three-dimensional (3D) geometries from two-dimensional (2D) images without any labeled information is promising for understanding the real world without incurring annotation cost. We herein propose a novel generative model, RGBD-GAN, which achieves unsupervised 3D representation learning from 2D images. The proposed method enables camera parameter conditional image generation and depth image generation without any 3D annotations such as camera poses or depth. We used an explicit 3D consistency loss for two RGBD images generated from different camera parameters in addition to the ordinal GAN objective. The loss is simple yet effective for any type of image generator such as the DCGAN and StyleGAN to be conditioned on camera parameters. We conducted experiments and demonstrated that the proposed method could learn 3D representations from 2D images with various generator architectures.

1 INTRODUCTION

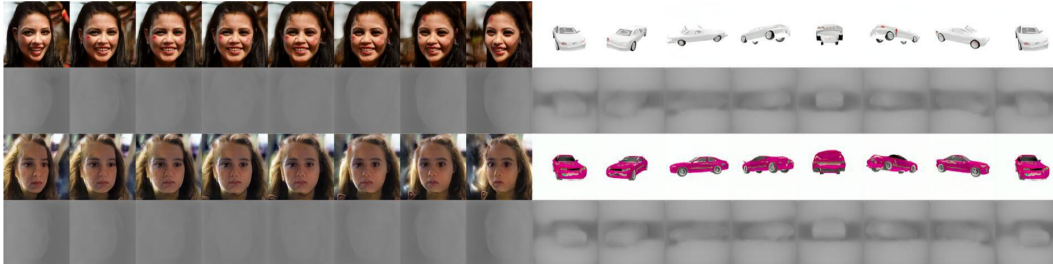


Figure 1: Generated RGBD images conditioned on camera parameters from StyleGAN. Gray images are generated depth images. The proposed method enables the joint distribution of RGB and depth to be learned and disentangles camera parameters from **unlabeled RGB** image datasets.

Understanding three-dimensional (3D) geometries from two-dimensional (2D) images is important in computer vision. An image of objects in the real world comprises two independent components: object identity and camera pose. Object identity represents the shape and texture of an object, and camera pose comprises camera rotation and translation, and intrinsics such as focal length. Learning the representation of these two components independently facilitates in understanding the real 3D world. For example, camera pose invariant feature extraction can facilitate object identification problems, and camera pose variant feature representations are beneficial for the pose estimation of the objects. These tasks are easy for humans but difficult for machines.

Recently, 3D representation learning through 3D object generation has been actively researched. Many techniques are available for learning the relationship between 2D images and 3D objects, which is called 3D object reconstruction from 2D images. Typically used 3D representations are voxel grids (Yan et al., 2016; Wu et al., 2016; Choy et al., 2016), point clouds (Fan et al., 2017), and meshes (Kato et al., 2018; Wang et al., 2018; Kato & Harada, 2019). For all methods, 3D annotations

such as ground truth 3D models (Choy et al., 2016; Fan et al., 2017; Wang et al., 2018), multiple-view images (Yan et al., 2016), or silhouette annotations of objects (Yan et al., 2016; Kato et al., 2018; Kato & Harada, 2019) must be used. Although these methods achieve 3D object generation by controlling the object identity and camera poses independently, the construction of such datasets requires considerable time and effort. Therefore, a method that can learn 3D representations without any labeled information must be developed. Furthermore, methods to generate high-resolution 3D objects with fidelity have not been developed owing to memory constraint or training instability.

To realize unsupervised 3D object generation, we employ a different approach, i.e., RGBD image synthesis. RGBD images comprise the color and depth information of each pixel. The proposed RGBD image synthesis can be achieved through a simple extension of recently developed image generation models. Recently, image generation models have shown significant progress, especially generative adversarial networks (GANs) (Goodfellow et al., 2014). A GAN adversarially trains a discriminator that estimates the distribution distance between generated and real images; additionally it trains a generator that minimizes the estimated distance. As such, the distribution of training images can be estimated precisely without supervision. Recent interests in generative models pertain to their training stability (Arjovsky et al., 2017; Gulrajani et al., 2017; Miyato et al., 2018) and improvement in quality and diversity (Karras et al., 2018; Brock et al., 2019; Karras et al., 2019). Furthermore, methods to learn 3D representation from 2D images by constructing a generative model conditioned on camera parameters have been proposed (Shen et al., 2018; Sitzmann et al., 2019; Nguyen-Phuoc et al., 2019). Shen et al. (2018) and Sitzmann et al. (2019) learned to generate images by controlling camera poses using camera pose annotations or images captured from multiple viewpoints. Although these methods can successfully control an object pose, the scalability is limited owing to the annotation costs. Nguyen-Phuoc et al. (2019) recently proposed a method to disentangle object identity and camera poses without any annotations. This method uses latent 3D features and learns to generate images from the feature projected from the 3D feature with rigid-body transformations. That is, this method uses strong inductive biases regarding the 3D world to learn the relationship between camera poses and images. Although this model can model the 3D world reasonably well, its 3D latent feature processing requires considerable memory and computational costs than 2D CNNs, thus limiting its scalability. Furthermore, these image generation models cannot output explicit 3D representations, thus limiting the understandability of the output.

We propose the RGBD-GAN, which learns to generate RGBD images from natural RGB image datasets without any annotations such as camera pose annotations, multiple viewpoints for single objects, and depth annotations. The proposed model uses an explicit 3D consistency loss for the generated images; the model generates two RGBD images with different camera parameters and learns them to be consistent with the 3D world. This training pipeline is simple yet effective for generating depth images without supervision and for disentangling a camera pose from the image content. Because the proposed model does not restrict the generator architecture, we can condition any type of image generator (e.g., PGGAN (Karras et al., 2018), StyleGAN (Karras et al., 2019)) on camera parameters. Figure 1 shows the generation results from the StyleGAN.

Our contributions are as follows.

- We propose a new image generation technique, i.e., RGBD image synthesis, which can be achieved from RGB images without any labeled information such as annotations of camera parameters, depth, or multiple viewpoints for single objects.
- The proposed method can disentangle camera parameters from the image content without any supervision.
- Our method can be used to condition any type of generator on camera parameters because the proposed loss function does not restrict the generator architecture.

2 METHOD

In this study, unsupervised 3D representation learning is achieved via RGBD image synthesis. The proposed method does not require any type of supervision such as annotations of camera parameters, depth, and multiple viewpoints for a single object. In this section, we first describe the motivation to use RGBD representation for unsupervised 3D representation learning in subsection 2.1; furthermore, we provide the details of our method in subsection 2.2.

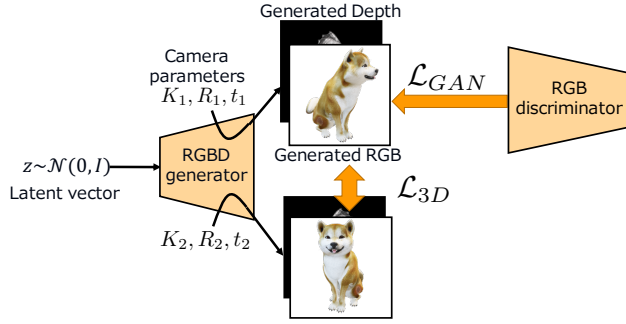


Figure 2: Proposed pipeline. We train the RGBD image generator with the self-supervised 3D consistency loss and adversarial loss for RGB channels.

2.1 MOTIVATION

A goal of this research is to construct a model that can generate images I conditioned on camera parameters c . However, it is impossible to perfectly model the relationship between c and I without any annotations. Therefore, we alleviate the problem by considering optical flow consistency. Although optical flow is typically used for two different frames in a movie, we used it for images captured with different camera parameters. Optical flow consistency is expressed as the pixel movement between two images.

$$I(x, y, c) = I(x + \Delta x, y + \Delta y, c + \Delta c) \quad \text{for } \forall x, y, c \quad (1)$$

Here, x and y are pixel coordinates in the image. Considering a small Δc , this equation can be written as the following partial differential equation.

$$\frac{\partial I}{\partial x} \frac{dx}{dc} + \frac{\partial I}{\partial y} \frac{dy}{dc} + \frac{\partial I}{\partial c} = 0 \quad \text{for } \forall x, y, c \quad (2)$$

$\frac{\partial I}{\partial x}$ and $\frac{\partial I}{\partial y}$ can be estimated using ordinary image generation models. Therefore, if $\frac{dx}{dc}$ and $\frac{dy}{dc}$ are known, then $\frac{\partial I}{\partial c}$ can be calculated. This term can be helpful for conditioning the generator on the camera parameters when optimizing the GAN objective. However, $\frac{dx}{dc}$ and $\frac{dy}{dc}$ are still unknown. Therefore, we alleviate this problem by considering a geometric constraint on a homogeneous coordinate. Let d be the depth, $p = (x, y, 1)$ the homogeneous coordinate of the pixel, p_{world} the world coordinate of the pixel, R the rotation matrix, t the translation vector, and K the camera intrinsics. The camera parameters c are represented herein as $\{K, R, t\}$. p_{world} is constant to c . At this time, we can calculate the position on an image and the depth from the world coordinate p_{world} .

$$dp = KRp_{world} + Kt \quad (3)$$

This facilitates in calculating $\frac{dx}{dc}$ and $\frac{dy}{dc}$ by estimating the depth d . Hence, we used the RGBD representation for camera parameter conditioning. For depth image d , an optical flow consistency as an RGB image exists, considering the camera parameter change. This facilitates in estimating the depth image d .

$$d(x, y, c) = d(x + \Delta x, y + \Delta y, c + \Delta c) + \Delta d \quad \text{for } \forall x, y, c \quad (4)$$

Here, Δd can be calculated from Equation 3.

Briefly, training a GAN with the constraints in Equation 1, 3, and 4 is beneficial for learning $\frac{\partial I}{\partial c}$, which benefits camera parameter conditional synthesis. Additionally, learning a camera parameter conditional image generation model facilitates in learning depth distributions with the constraint from Equation 1 and 3. The details for each module are explained below.

2.2 PROPOSED PIPELINE

The proposed model comprises three components: an RGBD image generator conditioned on camera parameters, RGB discriminator for adversarial training, and self-supervised RGBD consistency loss. The overview of the pipeline is shown in Figure 2.

2.2.1 RGBD GENERATOR

In the previous subsection, we showed that depth image estimation facilitates in learning the relationship between images and camera parameters. In this section, we explain the method for the RGBD image generator. Considering the success in image generation, the generator of a GAN can estimate complicated distributions. Therefore, we used ordinary RGB image generators such as the DCGAN or StyleGAN for RGBD synthesis. RGBD synthesis is achieved by adding one channel to the final layer of the RGB generator. Moreover, as described in the experimental section, we can use image generation models through 3D latent representations such as the HoloGAN (Nguyen-Phuoc et al., 2019), which models the 3D world more naturally.

In the proposed pipeline, the generator is conditioned on camera parameters and trained with the self-supervised consistency loss described in the next subsection. Because no constraint exists for the generator architecture, any type of generator architecture can be used for RGBD image synthesis, thus resulting in the high applicability of the method.

2.2.2 SELF-SUPERVISED RGBD CONSISTENCY LOSS

In section 2.1, we showed that the optical flow consistency for RGB and depth can facilitate in learning camera parameter conditional image generation. We approximated the constraint in Equation 1 and 4 by sampling two camera parameters c_1 and c_2 and minimizing the difference of both sides of the equations for two generated images conditioned on the camera parameters, where $c = c_1$ and $c + \Delta c = c_2$. In this study, the camera parameters are sampled from a predefined distribution $p(c)$ according to the dataset, similarly to the HoloGAN. We limit the maximum values of Δc to 30° to avoid large occlusion.

The objective function for Equation 1 is similar to the loss used in monocular video depth estimation (Zhou et al., 2017). Using Equation 3, we can calculate the 3D position of each pixel when an RGBD image is viewed from different viewpoints. Therefore, images captured from c_2 can be rendered by sampling the pixel values from RGBD images captured from c_1 . This operation is typically called the ‘‘warp’’ operation. The operation was implemented with bilinear sampling between the colors of four neighboring pixels of warped coordinates such that it was differentiable. We applied this loss to the generated RGBD images conditioned on c_1 and c_2 . The main difference between depth estimation and the proposed method is that our method optimizes both the RGB and depth image generator, although depth estimation only optimizes the depth estimator.

Moreover, for the constraints of the depth map in Equation 4, we define a consistency loss to the generated depth maps. This loss attempts to equate the depth map generated from c_1 in 3D space to that generated from c_2 , which is similar to the left–right disparity consistency loss in (Godard et al., 2017). The proposed 3D loss function can be written as Equation 5.

$$\begin{aligned} \mathcal{L}_{3D} = \mathbb{E}_{z \sim p(z), c_{1,2} \sim p(c)} [& \|G_{RGB}(z, c_1) - \text{warp}(G_{RGB}(z, c_2), c_{1 \rightarrow 2})\|_1^2 \\ & + \|\text{projection}(G_D(z, c_1), c_{1 \rightarrow 2}) - \text{warp}(G_D(z, c_2), c_{1 \rightarrow 2})\|_1^2 \end{aligned} \quad (5)$$

Here, $G_{RGB}(z, c)$ and $G_D(z, c)$ are the generated RGB and depth image from a latent vector z and camera parameters c respectively, and $c_{1 \rightarrow 2}$ is a relative transformation matrix from c_1 to c_2 . The ‘‘projection’’ operation calculates the depth value viewed from different viewpoints from the input depth map using Equation 3. The ‘‘Warp’’ operation is a bilinear resampling of the input images. For simplification, we omit the loss for the inverse transformation $c_{2 \rightarrow 1}$ in the equation.

This loss function causes inaccurate gradients for the occluded pixels during the transformation $c_{1 \rightarrow 2}$ because it does not consider those regions. Therefore, in this study, we used the occlusion aware consistency loss proposed in (Gordon et al., 2019). This technique propagates gradients only to pixels where the projected depth is smaller than the depth of the other viewpoint image. This prevents inaccurate gradients in pixels that move behind other pixels during projection.

Finally, we add a depth constraint term to stabilize the training. The loss above can be easily minimized to 0 when the generated depth is extremely small. Therefore, we set the minimum limit for the depth value as d_{min} and add a regularization for depth values smaller than d_{min} .

$$\mathcal{L}_{depth} = \sum_{x,y} \max(0, (d_{min} - d(x, y)))^2 \quad (6)$$

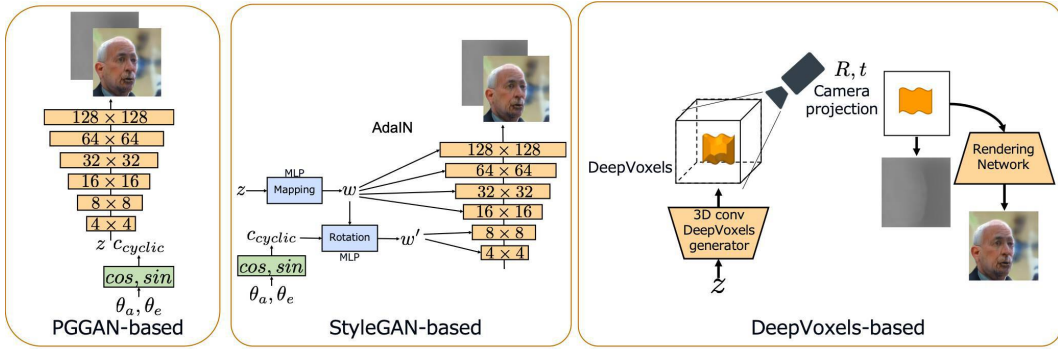


Figure 3: Generator architectures tested. PGGAN-based model (left), StyleGAN-based model (middle), and DeepVoxels-based model (right).

2.2.3 RGB DISCRIMINATOR

To achieve the training of an RGBD generator from unlabeled RGB images, we apply adversarial loss only for the RGB channels of generated images. Although the loss can only improve the reality of the images, this loss is beneficial for learning depth images and camera parameter conditioning through the optimization of the loss in Equation 5.

Based on the above, the final objective for the generator \mathcal{L}_G is as follows.

$$\mathcal{L}_G = \mathcal{L}_{GAN} + \lambda_{3D}\mathcal{L}_{3D} + \lambda_{depth}\mathcal{L}_{depth} \quad (7)$$

Here, \mathcal{L}_{GAN} is an adversarial loss function, and λ is a hyperparameter.

3 EXPERIMENTS

3.1 MODEL ARCHITECTURES

The proposed method does not restrict the generator architecture: any type of image generators can be conditioned on camera parameters. To demonstrate the effectiveness of our method, we tested three types of image generation models: PGGAN, StyleGAN, and DeepVoxels. The model architectures are shown in Figure 3. Because perspective information is difficult to obtain from a single image, in this experiment, the camera intrinsics K are fixed during training. We controlled only the azimuth θ_a (left–right rotation) and elevation θ_e (up–down rotation) parameters based on the training setting of the HoloGAN. In the following, we provide the details of each model architecture.

PGGAN: A PGGAN (Karras et al., 2018) is a state-of-the-art DCGAN. In this experiment, we conditioned the model on two camera parameters, azimuth and elevation, as follows: First, these values are input to \cos and \sin functions, respectively, and the outputs are concatenated to a single vector c_{cyclic} . Subsequently, the four-dimensional vector is concatenated to latent vector z , which is input to the generator. This operation allows the generated images to change continuously for a 360° angle change. We start with a resolution of 32×32 and increase it progressively to 128×128 .

StyleGAN: A StyleGAN (Karras et al., 2019) is a state-of-the-art GAN model that controls the output “style” of each convolutional layer by performing adaptive instance normalization (AdaIN) (Huang & Belongie, 2017) and acquires hierarchical latent representations. We used c_{cyclic} to only control the style of features on resolutions of 4×4 and 8×8 , as it is known that styles at low-resolution layers control global features such as the pose and shape of an object. More concretely, we concatenated c_{cyclic} and the output of the mapping network w , which was then converted to w' with a multilayer perceptron. Please refer to Figure 3. We start with a resolution of 32×32 and increase it to 128×128 progressively.

DeepVoxels: The HoloGAN enables the disentanglement of camera parameters by using 3D latent feature representations. This is a more natural and realistic modeling of the 3D world than the two models above because it considers explicit transformations in 3D space. However, the HoloGAN cannot consider depth information as the projection unit of the HoloGAN only calculates

the weighted sum of feature on the depth dimension. Therefore, we used the model inspired by DeepVoxels (Sitzmann et al., 2019) to apply the proposed method. DeepVoxels is a method that can learn the 3D latent voxel representation of objects using images from multiple viewpoints of a single object; additionally, it can generate novel-view images. This method uses the occlusion-aware projection module that learns which voxels are visible from the camera viewpoint along the depth axis. This is achieved via unsupervised learning. Therefore, a depth image can be acquired from the model, which is suitable for combining with our method. In this experiment, we combined DeepVoxels and a voxel feature generator that generates features from random latent vector z , to be used for the random image generation task. We used 3D convolution and AdaIN for the voxel feature generator, similarly to the HoloGAN. DeepVoxels uses an explicit camera model to acquire the feature visible in the camera frustum, whereas the HoloGAN uses rigid-body transformations. This enables a more accurate reasoning about the 3D world. Moreover, for simplicity, we did not use the Identity regulariser and style discriminator. We compare the three settings for the models using 3D feature representations. The first model uses the weighted sum of depth dimensions instead of occlusion-aware projection modules, similarly to the HoloGAN. The second model uses occlusion-aware projection modules but does not use the proposed 3D loss. The final model uses DeepVoxels and the proposed 3D loss. The methods are called “HoloGAN-like,” “DeepVoxels,” and “DeepVoxels + 3D loss” in the figures and tables. It is noteworthy that “HoloGAN-like” is not the same model as the original HoloGAN because it is based on DeepVoxels’ network structures.

3.2 DATASETS

We trained our model using FFHQ (Karras et al., 2019), cars from ShapeNet (Chang et al., 2015), car images (Krause et al., 2013), and the LSUN bedroom dataset (Yu et al., 2015). We used 128×128 images for the PGGAN and StyleGAN, and 64×64 images for models using 3D latent feature representations owing to memory constraints. We used 35° for the elevation angle range for all experiments, 120° for the azimuth range for the FFHQ and bedroom datasets, and 360° for the azimuth range for the Car and ShapeNet car datasets. For the ShapeNet car dataset, we used a new occlusion reasoning algorithm for DeepVoxels-based models to stabilize the training. The details are explained in the appendix.

3.3 RESULTS

Qualitative results The generative results from each model controlling the camera parameters on the FFHQ and ShapeNet car datasets are shown in Figures 4 and 5. In the figures, gray images show the generated depth images. The depth is visualized as black when the depth value is large. For all models using the proposed loss (top three in the figures), images can be generated by controlling the camera parameters, preserving their identity. Moreover, the models can generate depth images that do not exist in the training samples. To confirm the depth consistency, we showed normal maps and rotated images for the generative results from the StyleGAN, as shown in Figure 6. The white regions of the ShapeNet car dataset are omitted for the visualization of point clouds. As shown in the figure, the models can generate the convex shape of a face and the rectangular shape of a car without any annotations regarding the 3D world. In particular, although the PGGAN and StyleGAN use the 2D CNN, consistent rotation and depth estimation are achieved, which is impossible with previous methods. This implies that the proposed method has good generalization performance on the generator architecture. The DeepVoxels-based method with the proposed loss performs well on both FFHQ and the ShapeNet car dataset. They can acquire more consistent rotation and generate more consistent depth images than 2D CNN-based models. This is thanks to the explicit 3D modeling about 3D space, though it does consume much memory and has high computational cost.

For the ShapeNet car dataset in Figure 5, PGGAN- and StyleGAN-based methods can generate consistently rotated images. However, for the PGGAN, only a 180° azimuth change is acquired. This is because the model cannot distinguish between the front and back of the car, as it is difficult to achieve only with unsupervised learning. Meanwhile, StyleGAN-based methods can learn consistent azimuth and elevation angle changes. This is because the StyleGAN is stable owing to its hierarchical latent representation.

Comparing three 3D-latent-feature-based methods for the datasets, “HoloGAN-like” method works well on the FFHQ dataset but cannot acquire consistent 360° rotation on the ShapeNet car dataset



Figure 4: Visualization of comparison for the generated images from each model on FFHQ dataset. Images in each row are generated from the same latent vector z but different azimuth or elevation angles. The grayscale images are the generated depth images.

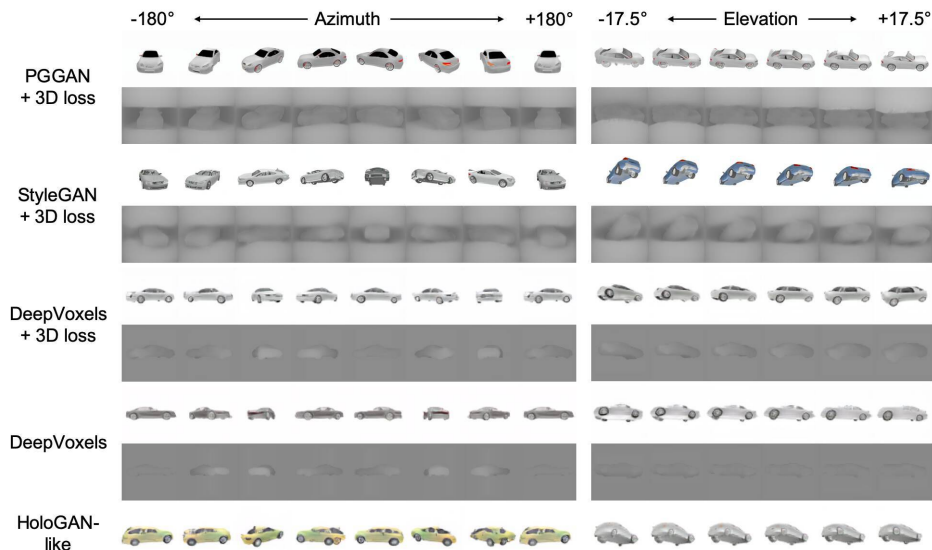


Figure 5: Visualization of comparison for the generated images from each model on ShapeNet car images. Images in each row are generated from the same latent vector z but different azimuth or elevation angles. The grayscale images are generated the depth images.

in our training settings. DeepVoxels-based methods, on the other hand, can control 360° object rotation on the dataset, realizing the depth map generation without any supervised information. This result shows that the depth reasoning helps to generate images considering the 3D geometry of the objects. Moreover, DeepVoxels-based method with the proposed loss can generate more consistent images for the FFHQ dataset. For example, in “DeepVoxels”, the depth of the background is smaller than that of the face; however, this does not occur when the proposed loss is used. This is because our method considers warped images from different viewpoints, thus facilitating the model to accurately learn the 3D world.

Moreover, additional generative results from the StyleGAN on the car image and bedroom datasets are shown in Figure 7. For the dataset preprocessing, we center cropped the images without aligning

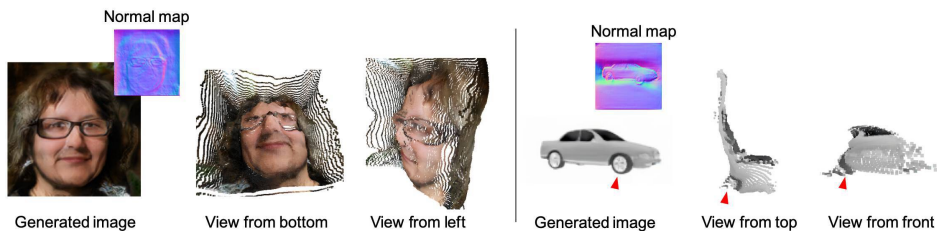


Figure 6: Normal map and point cloud visualization for FFHQ and ShapeNet car datasets. Point clouds in occluded region are not visualized in the figure. We show the placemarks for the tire for better understanding.

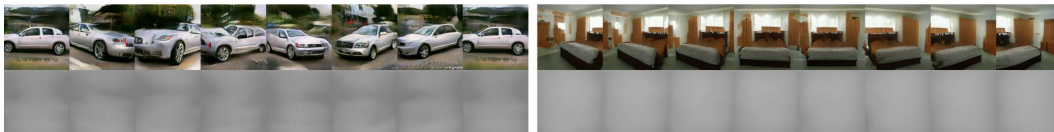


Figure 7: Generated car and bedroom images using the StyleGAN with proposed loss changing the azimuth angle range.

Table 1: Performance comparison of unconditional generation models and proposed camera parameter conditional models. We report FID for each model.

MODEL	FFHQ	ShapeNet Car
PGGAN	28.5	16.7
PGGAN + 3D loss	30.3	14.5
StyleGAN	20.9	15.5
StyleGAN + 3D loss	24.2	13.5
HoloGAN-like	23.4	33.5
DeepVoxels	19.4	28.6
DeepVoxels + 3D loss	21.1	31.2

the object position. Despite the diversity of the camera poses and object layouts, the model could learn to generate images by controlling the camera poses.

As a result, the proposed method effectively helps the generators to learn both depth information and explicit controls on camera poses. These are achieved without the need for 3D latent representations as HoloGAN does, and moreover, the proposed method further improve the results for the models using 3D latent representations.

Quantitative results We compared the Frchet inception distance (FID) (Heusel et al., 2017) between models with and without the proposed method for each generator architecture. FID is a typical evaluation metric for image generation models. The results are shown in Table 1. The results show that the proposed camera parameter conditional image generation models can generate images with competitive or even better FIDs than unconditional or RGB image generation models for all types of generator architectures. The results show the robustness and effectiveness of our method against the architectures of the generator.

4 CONCLUSION

We herein proposed an RGBD image synthesis technique for camera parameter conditional image generation. Although the proposed method did not require any labeled dataset, it could explicitly control the camera parameters of generated images and generate consistent depth images. The method did not limit the generator architecture, and could be used to condition any type of image generator on camera parameters. As the proposed method could learn the relationship between camera parameters and images, future works will include extending the method for unsupervised camera pose estimation and unsupervised camera pose invariant feature extraction from images.

5 ACKNOWLEDGEMENT

This work was partially supported by JST CREST Grant Number JPMJCR1403, and partially supported by JSPS KAKENHI Grant Number JP19H01115. We would like to thank Antonio Tejero de Pablos, Dexuan Zhang, Hiroaki Yamane, James Borg, Takayuki Hara, and Toshihiko Matsuura for helpful discussions.

REFERENCES

- Martin Arjovsky, Soumith Chintala, and Léon Bottou. Wasserstein generative adversarial networks. In *ICML*, 2017.
- Andrew Brock, Jeff Donahue, and Karen Simonyan. Large scale gan training for high fidelity natural image synthesis. In *ICLR*, 2019.
- Angel X Chang, Thomas Funkhouser, Leonidas Guibas, Pat Hanrahan, Qixing Huang, Zimo Li, Silvio Savarese, Manolis Savva, Shuran Song, Hao Su, et al. Shapenet: An information-rich 3d model repository. *arXiv preprint arXiv:1512.03012*, 2015.
- Christopher B Choy, Danfei Xu, JunYoung Gwak, Kevin Chen, and Silvio Savarese. 3d-r2n2: A unified approach for single and multi-view 3d object reconstruction. In *ECCV*. Springer, 2016.
- Haoqiang Fan, Hao Su, and Leonidas J Guibas. A point set generation network for 3d object reconstruction from a single image. In *CVPR*, 2017.
- Clément Godard, Oisín Mac Aodha, and Gabriel J Brostow. Unsupervised monocular depth estimation with left-right consistency. In *CVPR*, 2017.
- Ian J Goodfellow, Jean Pouget-Abadie, Mehdi Mirza, Bing Xu, David Warde-Farley, Sherjil Ozair, Aaron Courville, and Yoshua Bengio. Generative Adversarial Nets. In *NIPS*, 2014.
- Ariel Gordon, Hanhan Li, Rico Jonschkowski, and Anelia Angelova. Depth from videos in the wild: Unsupervised monocular depth learning from unknown cameras. *arXiv preprint arXiv:1904.04998*, 2019.
- Ishaan Gulrajani, Faruk Ahmed, Martin Arjovsky, Vincent Dumoulin, and Aaron C Courville. Improved training of wasserstein gans. In *NIPS*, 2017.
- Martin Heusel, Hubert Ramsauer, Thomas Unterthiner, Bernhard Nessler, and Sepp Hochreiter. Gans trained by a two time-scale update rule converge to a local nash equilibrium. In *NIPS*, 2017.
- Xun Huang and Serge J Belongie. Arbitrary style transfer in real-time with adaptive instance normalization. In *ICCV*, 2017.
- Tero Karras, Timo Aila, Samuli Laine, and Jaakko Lehtinen. Progressive Growing of GANs for Improved Quality, Stability, and Variation. In *ICLR*, 2018.
- Tero Karras, Samuli Laine, and Timo Aila. A style-based generator architecture for generative adversarial networks. In *CVPR*, 2019.
- Hiroharu Kato and Tatsuya Harada. Learning view priors for single-view 3d reconstruction. In *CVPR*, 2019.
- Hiroharu Kato, Yoshitaka Ushiku, and Tatsuya Harada. Neural 3d mesh renderer. In *CVPR*, 2018.
- Jonathan Krause, Michael Stark, Jia Deng, and Li Fei-Fei. 3d object representations for fine-grained categorization. In *4th International IEEE Workshop on 3D Representation and Recognition (3dRRR-13)*, Sydney, Australia, 2013.
- Lars Mescheder, Andreas Geiger, and Sebastian Nowozin. Which training methods for gans do actually converge? In *ICML*, 2018.
- Takeru Miyato, Toshiki Kataoka, Masanori Koyama, and Yuichi Yoshida. Spectral normalization for generative adversarial networks. In *ICLR*, 2018.

- Thu Nguyen-Phuoc, Chuan Li, Lucas Theis, Christian Richardt, and Yong-Liang Yang. Hologan: Unsupervised learning of 3d representations from natural images. 2019.
- Yujun Shen, Ping Luo, Junjie Yan, Xiaogang Wang, and Xiaoou Tang. Faceid-gan: Learning a symmetry three-player gan for identity-preserving face synthesis. In *CVPR*, 2018.
- Vincent Sitzmann, Justus Thies, Felix Heide, Matthias Nießner, Gordon Wetzstein, and Michael Zollhofer. Deepvoxels: Learning persistent 3d feature embeddings. In *CVPR*, 2019.
- Nanyang Wang, Yinda Zhang, Zhuwen Li, Yanwei Fu, Wei Liu, and Yu-Gang Jiang. Pixel2mesh: Generating 3d mesh models from single rgb images. In *ECCV*, 2018.
- Jiajun Wu, Chengkai Zhang, Tianfan Xue, Bill Freeman, and Josh Tenenbaum. Learning a probabilistic latent space of object shapes via 3d generative-adversarial modeling. In *NIPS*, 2016.
- Xinchen Yan, Jimei Yang, Ersin Yumer, Yijie Guo, and Honglak Lee. Perspective transformer nets: Learning single-view 3d object reconstruction without 3d supervision. In *NIPS*, 2016.
- Fisher Yu, Ari Seff, Yinda Zhang, Shuran Song, Thomas Funkhouser, and Jianxiong Xiao. Lsun: Construction of a large-scale image dataset using deep learning with humans in the loop. *arXiv preprint arXiv:1506.03365*, 2015.
- Tinghui Zhou, Matthew Brown, Noah Snavely, and David G Lowe. Unsupervised learning of depth and ego-motion from video. In *CVPR*, 2017.

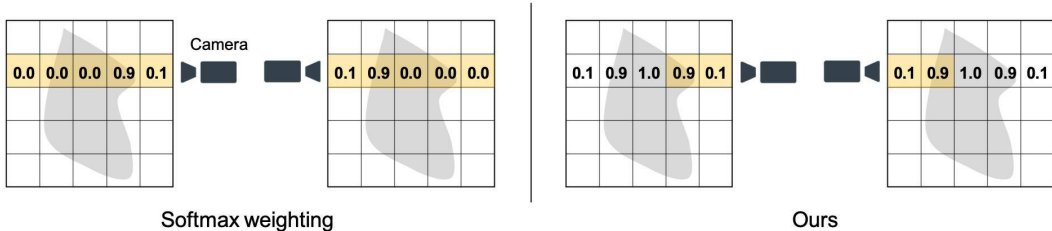


Figure 8: Comparison between the softmax weighting (left) and our occlusion reasoning algorithm (right). The values are the weight for each voxel. Our method accumulates the weight along the camera ray and ignores the voxels where the accumulative values exceed one. The orange regions are visible voxels from the camera.

A CAMERA PARAMETER DISTRIBUTIONS

To randomly sample two similar camera parameters c_1 and c_2 , we first sample c_1 from a uniform distribution and then sample c_2 from an area near to c_1 within the angle range. We limit the maximum distance between c_1 and c_2 as 30° to avoid large occlusions.

B IMPLEMENTATION DETAILS FOR DEEPVOXELS

The components we used to implement the DeepVoxels-based methods were the projection layer, occlusion module, and rendering module, which are proposed in (Sitzmann et al., 2019). We implemented them with structures simpler than those of the original implementation to reduce the computational costs and memory usage. We used fewer 3D convolutional layers for occlusion module and a U-Net-like network with AdaIN for the rendering module.

For occlusion reasoning, we used a different algorithm to learn more consistent depth for the ShapeNet car datasets. The occlusion reasoning to get image features used in DeepVoxels is softmax weighting along the depth axis, which is visualized on the left side of Figure 8. This algorithm needs the occlusion module to calculate the weight of the voxels according to the camera poses, which is very difficult through unsupervised learning. Therefore, to reduce the training cost of the occlusion network, we use a more explicit reasoning algorithm. First, the network estimates the probability of



Figure 9: Comparison of the occlusion reasoning algorithms. The proposed method can acquire more consistent rotation and generate consistent depth maps than the softmax weighting.

each voxel to be on the surface of the object or not; i.e. the opacity of each voxel. This is implemented with a sigmoid activation function. Then, the weights are accumulated along the rays from the camera by summing the values, and when the accumulated values exceed 1, the later voxels are ignore, i.e., the weight values are replaced with 0s. The algorithm overview is shown in the right side of Figure 8.

We show the generative results from “DeepVoxels + 3D loss” with each algorithm in Figure 9. The model that uses the proposed occlusion reasoning can acquire more consistent 360° rotation, whereas the softmax weighting cannot. Moreover, the proposed algorithm can generate consistent depth maps compared to the softmax weighting. The results show the effectiveness of the proposed method for unsupervised learning.

C TRAINING DETAILS

We trained PGGAN- and StyleGAN-based models for 300,000 iterations with batchsize 32, and 3D-latent-feature-based models for 75,000 iterations with batchsize 10. All models are trained with Adam optimizer with learning rate 0.001 for the generators, 0.00001 for the mapping networks, and 0.003 for the discriminators. In the experiments, we used a ResNet-based discriminator and nonsaturating loss (Goodfellow et al., 2014) with gradient penalty (Mescheder et al., 2018).